



General approach of terahertz achromatic quarter-wave plate composed of stacked quartz plates

TIANMIAO ZHANG, GRIGORY KROPOTOV,
AND MIKHAIL KHODZITSKY*

Department of Research and Development, Tydex LLC, Domostroitelnaya ulitsa 16B, Saint Petersburg 194292, Russian Federation

*khodzitskiy@yandex.ru

Abstract: Typical waveplates are limited to specific frequencies. We propose a general design of a series of THz achromatic quarter-wave plates that work for different frequency range. The simplified formulas and the basic parameters that are used to calculate the thicknesses and rotating angles with the possibility of choosing the frequency range are provided. The main feature of the design is that the number of the x-cut quartz plates is equal to the frequency expansion factor (f_{max}/f_{min}) of the resulting waveplate, and by altering the thicknesses of quartz plates following a specific pattern only, the frequency range of the waveplate can be shifted. Two achromatic waveplates working in the frequency range of 0.2-0.6 THz and 0.2-1.2 THz were manufactured for testing. The measurement result demonstrates the reliability of the proposed design.

© 2023 Optica Publishing Group under the terms of the [Optica Open Access Publishing Agreement](#)

1. Introduction

Terahertz (THz) time-domain spectroscopy (THz TDS) has increasingly gathered attention across various fields. Primarily, THz TDS is employed for the investigation of optical properties, such as complex refractive index, absorption coefficient, complex permittivity, complex conductivity of an object [1]. However, the exploration of polarization, another important characteristic of electromagnetic waves, has received comparatively less focus in THz TDS. To investigate polarization property of an object, THz time-domain polarimetry (THz TDP) is introduced by integration of a set of polarization converters and waveplates into conventional THz TDS [2]. The typical waveplates are made from birefringent materials and exhibit retardation properties influenced by the thicknesses, limiting their utility to specific frequencies. However, THz TDP inherits the broadband capabilities from THz TDS, necessitating the usage of THz achromatic waveplates as essential components.

Several approaches have been made to develop THz achromatic waveplates, such as silicon grating [3], stacked parallel metal plates [4], polymer composites with birefringence [5], liquid crystal [6], and metamaterials [7]. THz achromatic half- and quarter-wave plates using internal total reflection in a prism were also demonstrated [8]. Nonetheless, these approach either are complicated to be fabricated, or only cover narrow frequency range. Many designs of THz achromatic waveplates consisting of quartz plates with optical contact bonding were also proposed [9–12]. The waveplates with such composition are much easier to be manufactured and has the potential to extend the frequency range. However, these works didn't provide a general approach for other frequency ranges.

In this article we present the design and experiment results of a series of THz achromatic quarter-wave plates (AQW) that work for different frequency range. The idea is originally based on an article proposing an AQW consisting of a quartz plate and a MgF₂ plate for infrared wave [13]. We designed the THz AQW of the same composition by calculating the thickness L and the rotating angle θ of each plate [14]. The frequency expansion factor of the resulting AQW

is $FE = f_{max}/f_{min} = 2$. f_{max} and f_{min} are the frequencies where the retardation is at most 3% away from the target retardation of $\pi/2$. The retardation δ of a monochromatic waveplate can be described by the following formula: $\delta = 2\pi(n_o - n_e)L/\lambda_0$, where L is the thickness of the waveplate, λ_0 is the wavelength, and n_o and n_e are the ordinary and extraordinary refractive indices, respectively. As long as the difference between n_o and n_e is relatively a constant throughout the frequency range, MgF₂ and quartz are interchangeable by changing the thickness only. Therefore, the previously proposed AQW may also be achieved by 2 quartz plates. Moreover, a THz AQW consisting of 6 stacked quartz plates were proposed by J.B. Masson and G. Gallot [11]. Nonetheless, the FE of is not 7 as claimed by the authors. The actual FE, according to our simulation, is less than 6.5. After running several simulations of the designs above with different thicknesses and rotating angles, we noticed two features, that 1) the FE always equals to the quantity of the quartz plates that were used, and 2) the frequency range can be shifted by applying a coefficient to the predetermined base thicknesses. Therefore, the designs above are feasible to be further extended to improve the customizability of the THz AQW. Our goal is to propose a more general design consisting of 2-6 quartz plates that, consequently, possess the FEs of 2-6.

2. Design and simulation

A single quartz plate can be described by its Jones matrix [11,15]

$$J(\delta, \theta) = \begin{bmatrix} \cos \frac{\delta}{2} + i \cos 2\theta \sin \frac{\delta}{2} & i \sin 2\theta \sin \frac{\delta}{2} \\ i \sin 2\theta \sin \frac{\delta}{2} & \cos \frac{\delta}{2} - i \cos 2\theta \sin \frac{\delta}{2} \end{bmatrix}, \quad (1)$$

where δ, θ are the retardation and the rotating angle of the plate, respectively. The Jones matrix of the whole waveplate is obtained by multiplying all the matrices of each plate in order [11]. Thus, the key to extend the design is to find the pattern of δ and θ for each FE.

First, we started from the known designs of $FE = 2$ and $FE = 6$. We noticed that there is a pattern behind the thicknesses which are similar to the "greatest common divisor" for each design. We used simulated annealing (SA) to find out the thickness patterns for $FE = 3$, $FE = 4$ and $FE = 5$. SA is a generic algorithm of finding the parameters for a system to reach its most optimal status [16], and it has been widely used in many fields, including the design of AQW [11]. Since most of the elements in the pattern are integer 1 and 2, only the multiples of 0.5 and 1 were set to be search for the thickness pattern. The search of angles was limited to 2 decimal places in rad. After searching and optimizations using SA, the results are optimized to minimized the difference between the retardation of the AQW and the ideal retardation of $\pi/2$ down to $\pm 3\%$. Figure 1 shows the simulation of the AQWs consisting of 2 quartz plates with the FE of 2 while the frequency range is movable. This can be achieved by changing the thicknesses simultaneously. Figure 2 demonstrates the retardation simulations of the AQWs consisting of 2-6 quartz plates. The numbers in the brackets indicate the quantity of the quartz plates which is equal to the FE of each AQW.

Therefore, the more general design was proposed and can be described by the following equations:

$$FE = \frac{f_{max}}{f_{min}} = n_{plate}, \quad (2)$$

where FE is the frequency expansion factor, f_{max} and f_{min} are the frequencies where the retardation is at most 3% away from the target retardation of 0.5., n_{plate} is the number of quartz plates.

$$D_i = \frac{k}{f_{min}} \cdot d_i, \quad (3)$$

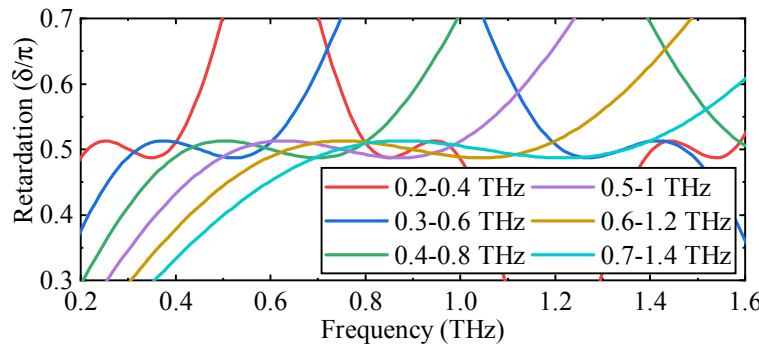


Fig. 1. The frequency range of the AQWs is movable while maintain the FE of 2. This can be achieved by changing all the thicknesses simultaneously.

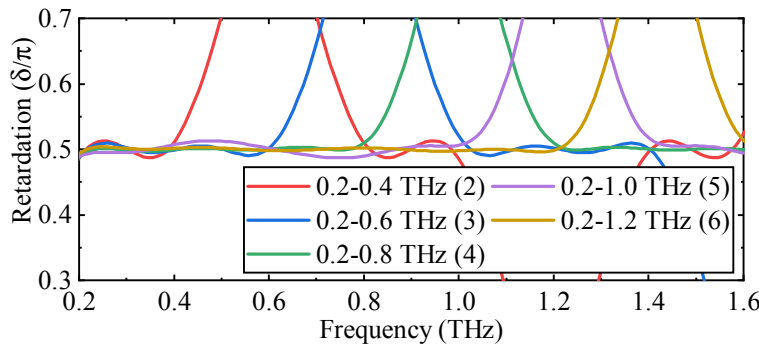


Fig. 2. The retardations of the AQWs consisting of 2-6 quartz plates. The numbers in the brackets indicate the quantity of the quartz plates which is equal to the FE of each AQW.

where D_i is the thickness of the i^{th} plate, d_i is the base thickness of the i^{th} plate, k is the coefficient depending on the number of quartz plates. The base thicknesses and the coefficients for all THz AQWs consisting of 2-6 quartz plates are given in the Table 1, Table 2, Table 3, Table 4 and Table 5.

Table 1. Parameters of AQW with FE = 2

2 plates	1	2
base thickness d (mm)	2	1
rotating angle θ (rad)	0.26	1.24
coefficient (THz)	1.07	

Table 2. Parameters of AQW with FE = 3

3 plates	1	2	3
base thickness d (mm)	2	2	1
rotating angle θ (rad)	0.17	0.65	1.8
coefficient (THz)	0.79		

Table 3. Parameters of AQW with $FE = 4$

4 plates	1	2	3	4
base thickness d (mm)	1	1	1	2.5
rotating angle θ (rad)	1.23	1.88	2.08	3.71
coefficient (THz)		1.28		

Table 4. Parameters of AQW with $FE = 5$

5 plates	1	2	3	4	5
base thickness d (mm)	1	2	1	1	2.5
rotating angle θ (rad)	0.53	0.06	1.91	0.02	1.2
coefficient (THz)		1.05			

Table 5. Parameters of AQW with $EF = 6$

6 plates	1	2	3	4	5	6
base thickness d (mm)	1	2	2	1	1	2.5
rotating angle θ (rad)	0.55	0.17	2.07	0.43	0.09	1.2
coefficient (THz)		0.9				

3. Experiment and evaluation

To evaluate the reliability of the proposed general design, we manufactured two AQW working at the frequency range of 0.2 – 0.6 THz and 0.2 – 1.2 THz with the parameters obtained from Table 2 and Table 5. For instance, for the 0.2 – 0.6 THz AQW, the thicknesses are $D = 0.79/0.2 \cdot [2 \ 2 \ 1]$, and the rotating angles are $\theta = [0.17 \ 0.65 \ 1.8]$, for the 0.2 – 1.2 THz AQW, the thicknesses are $D = 0.9/0.2 \cdot [1 \ 2 \ 2 \ 1 \ 1 \ 2.5]$, and the rotating angles are $\theta = 0.79/0.2 \cdot [1 \ 2 \ 2 \ 1 \ 1 \ 2.5]$.

The THZ TDP was used to measure the ellipticity angles and the transmittance of the AQWs. The experiment setup was built by a conventional THz time-domain spectroscope (TDS) employing 3 polarizers. Two photoconductive antennas were used as the THz emitter and detector. A square-wave generator was used as the modulator for the antennas and a lock-in amplifier is used to detect the current from the THz detector. The output power of the femtosecond laser is 260 mW and the pulse width is up to 90 fs. The dynamic range of the THz TDS is up to 70 (@ 0.5 THz). The scheme of the THz TDP setup is shown in Fig. 3. Two THz focus lenses were positioned after and before the emitter and detector to provide collimated parallel THz beam. The AQW and three polarizers were placed between the lenses. The first polarizer ensured that the linearly polarized THz beam was incident on the AQW. The second polarizer called "the analyzer" can be rotated and is placed after the AQW. The third polarizer is positioned after the AQW and its orientation is the same as the first polarizer.

Two measurements were carried out for each AQW to obtain the ellipticity angle. The analyzer was rotated by 45 and -45 (315) degrees relative to the orientation of the initial polarization. The exiting time-resolved electric fields \bar{E}_{45} and \bar{E}_{315} were recorded to be investigated. The ellipticity angle ϕ and retardation δ of the waveplate can be calculated using the following formulas [15]:

$$\bar{E}_x = \bar{E}_{45} + \bar{E}_{315}, \quad (4)$$

$$\bar{E}_y = \bar{E}_{45} - \bar{E}_{315}, \quad (5)$$

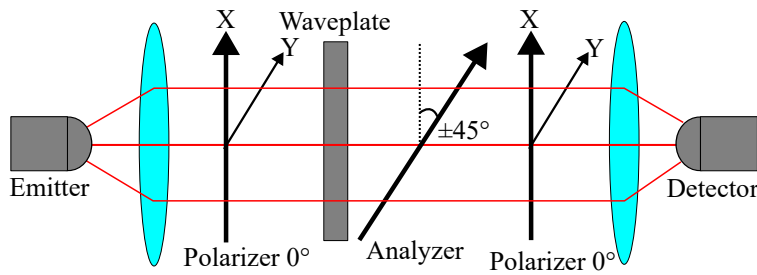


Fig. 3. The scheme of THz time-domain polarimetry setup. Two THz focus lenses were positioned after and before the emitter and detector to provide collimated parallel THz beam. The AQW and three polarizers were placed between the lenses. The first polarizer ensured that the linearly polarized THz beam was incident on the AQW. The second polarizer called "the analyzer" can be rotated and is placed after the AQW. The third polarizer is positioned after the AQW and its orientation is the same as the first polarizer.

$$\phi = \frac{1}{2} \sin^{-1} \frac{2\Im(\bar{E}_x \cdot \bar{E}_y^*)}{|\bar{E}_x|^2 + |\bar{E}_y|^2}, \quad (6)$$

$$\delta = 2 \cdot \tan^{-1} \sqrt{\frac{\Im^2(\bar{E}_x) + \Im^2(\bar{E}_y)}{\Re^2(\bar{E}_x) + \Re^2(\bar{E}_y)}}. \quad (7)$$

For the transmittance, two measurements were also carried out for each AQW. The polarizers were rotated back to 0 degree. One measurement was done without the AQW as the reference signal \bar{E}_{air} , and another measurement was done with the AQW as the sample signal \bar{E}_{sam} . Since the receiver of the TDS is sensitive to linear polarization, the transmittance can not be calculated directly by dividing the sample signal by the reference signal. According to the Jones calculus, when a circularly polarized beam goes through a linear polarizer, the output can be described as

$$\begin{pmatrix} 1 & 0 \\ 0 & 0 \end{pmatrix} \frac{1}{\sqrt{2}} \begin{pmatrix} 1 \\ -i \end{pmatrix} = \frac{1}{\sqrt{2}} \begin{pmatrix} 1 \\ 0 \end{pmatrix}. \quad (8)$$

The amplitude of the output electric field is $\frac{1}{\sqrt{2}}$ times smaller than that of the circularly polarized incident beam. Thus, the transmittance T of the AQW can be obtained by the following formula:

$$T = \sqrt{2} \frac{|\bar{E}_{sam}|}{|\bar{E}_{air}|}. \quad (9)$$

4. Results

The ellipticity angle of AQW for 0.2 – 0.6 THz (FE=3) and 0.2 – 1.2 THz (FE=6) are presented in Fig. 4 and Fig. 5, respectively. The experiment data (red curve) closely matches theoretical simulation (black curve) from Eq. (6).

The retardation of AQW for 0.2 – 0.6 THz (FE=3) and 0.2 – 1.2 THz (FE=6) are shown in Fig. 6 and Fig. 7. The oscillation appeared on the experiment data (red curve) may be caused by the reflections between the quartz plates. The simulation data is obtained from Eq. (7).

Although the performance of 0.2 – 1.2 THz AQW is slightly better than that of 0.2 – 0.6 THz AQW, due to its flatter retardation in the simulation, its transmittance is moderately less since its total thickness is greater, as shown in Fig. 8. The transmittance decreases with the increase of the frequency due to absorption of quartz [17]. The minimum transmittance is 40%.

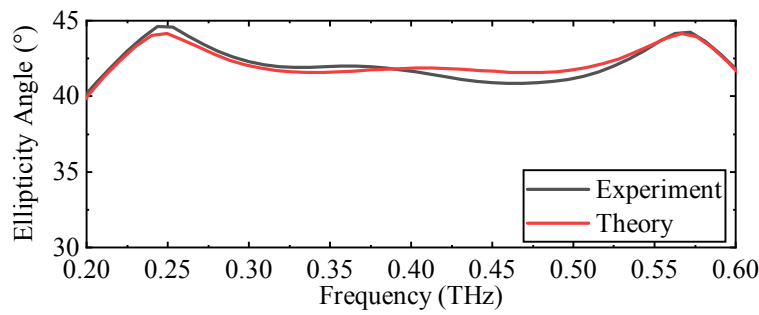


Fig. 4. The ellipticity angle (black line) of the AQW for 0.2 – 0.6 THz. The comparison with the simulation (red line) is also presented.

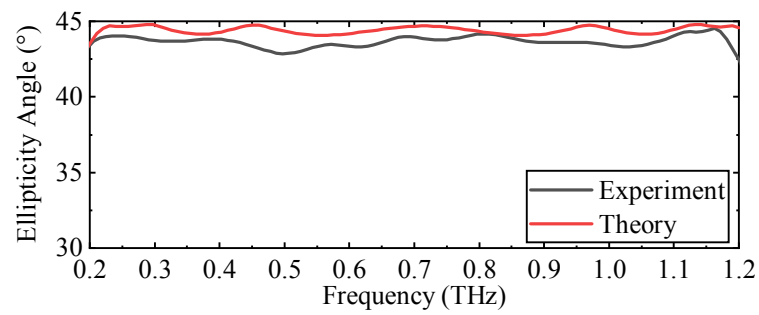


Fig. 5. The ellipticity angle (black line) of the AQW for 0.2 – 1.2 THz. The comparison with the simulation (red line) is also presented.

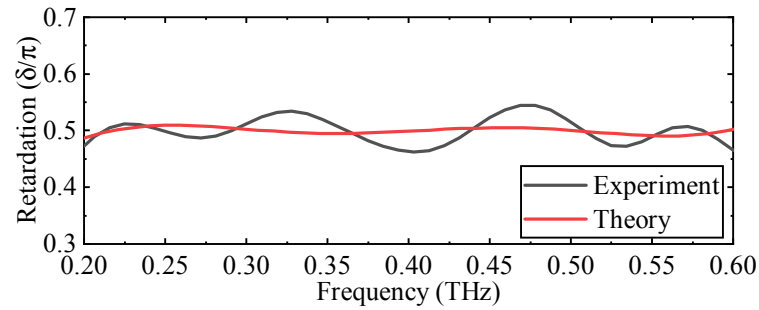


Fig. 6. The retardation (black line) of the AQW for 0.2 – 0.6 THz. The comparison with the simulation (red line) is also presented.

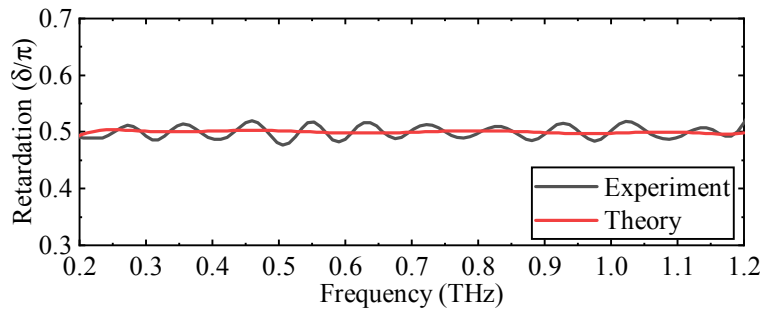


Fig. 7. The retardation (black line) of the AQW for 0.2 – 1.2 THz. The comparison with the simulation (red line) is also presented.

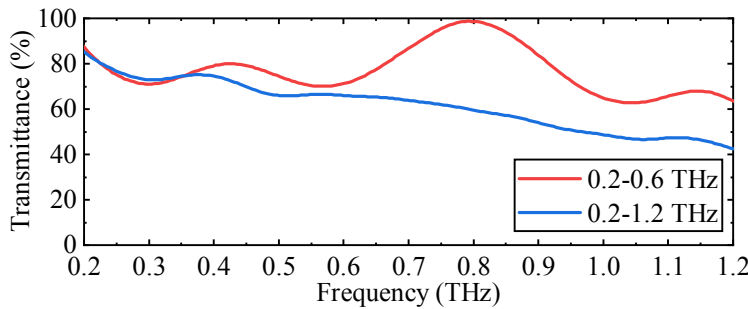


Fig. 8. The transmittance of the AQW for 0.2 - 0.6 THz (FE = 3, red line) and 0.2 - 1.2 THz (FE = 6, blue line).

5. Conclusion

In summary, we extended the design of terahertz achromatic quarter-wave plate and the reliability of the theory was evaluated and proved by the experiments by using THz time-domain polarimetry. We also provided the simplified formulas and parameter tables to calculate the thicknesses and rotating angles. The frequency expansion of the AQW is corresponding to the quantity of the quartz plates. The working frequency range can be altered by multiplying a coefficient associated with the minimum frequency. All the features above provide the high customizability of the THz AQW in varies frequency range.

Acknowledgments. This work was performed using the resources of Tydex LLC.

Disclosures. The authors declare no conflicts of interest.

Data availability. Data underlying the results presented in this paper are not publicly available at this time but may be obtained from the authors upon reasonable request.

References

1. M. C. Nuss and J. Orenstein, "Terahertz time-domain spectroscopy," *Millimeter and submillimeter wave spectroscopy of solids* pp. 7–50 (2007).
2. Y. Gong, Z. Zhang, K. Li, and W. Ren, "Review on polarimetric terahertz spectroscopy," *Microw. Opt. Technol. Lett.* **63**(6), 1605–1611 (2021).
3. B. Zhang and Y. Gong, "Achromatic terahertz quarter waveplate based on silicon grating," *Opt. Express* **23**(11), 14897–14902 (2015).
4. M. Nagai, N. Mukai, Y. Minowa, M. Ashida, J. Takayanagi, and H. Ohtake, "Achromatic thz wave plate composed of stacked parallel metal plates," *Opt. Lett.* **39**(1), 146–149 (2014).
5. X. Zhang, F. Fan, C.-Y. Zhang, Y.-Y. Ji, X.-H. Wang, and S.-J. Chang, "Tunable terahertz phase shifter based on dielectric artificial birefringence grating filled with polymer dispersed liquid crystal," *Opt. Mater. Express* **10**(2), 282–292 (2020).
6. C.-F. Hsieh, C.-S. Yang, F.-C. Shih, R.-P. Pan, and C.-L. Pan, "Liquid-crystal-based magnetically tunable terahertz achromatic quarter-wave plate," *Opt. Express* **27**(7), 9933–9940 (2019).
7. L. Cong, N. Xu, J. Gu, R. Singh, J. Han, and W. Zhang, "Highly flexible broadband terahertz metamaterial quarter-wave plate," *Laser Photonics Rev.* **8**(4), 626–632 (2014).
8. Y. Kawada, T. Yasuda, A. Nakanishi, K. Akiyama, K. Hakamata, and H. Takahashi, "Achromatic prism-type wave plate for broadband terahertz pulses," *Opt. Lett.* **39**(9), 2794–2797 (2014).
9. A. Kaveev, G. Kropotov, D. Tsypishka, I. Tzibizov, I. Vinerov, and E. Kaveeva, "Tunable wavelength terahertz polarization converter," in *2014 39th International Conference on Infrared, Millimeter, and Terahertz waves (IRMMW-THz)*, (IEEE, 2014), p. 1.
10. A. Kaveev, G. Kropotov, D. Tsypishka, I. Tzibizov, I. Vinerov, and E. Kaveeva, "Tunable wavelength terahertz polarization converter based on quartz waveplates," *Appl. Opt.* **53**(24), 5410–5415 (2014).
11. J.-B. Masson and G. Gallot, "Terahertz achromatic quarter-wave plate," *Opt. Lett.* **31**(2), 265–267 (2006).
12. Z. Chen, Y. Gong, H. Dong, T. Notake, and H. Minamide, "Terahertz achromatic quarter wave plate: Design, fabrication, and characterization," *Opt. Commun.* **311**, 1–5 (2013).
13. W. J. Rosenberg and A. M. Title, "Achromatic retardation plates," in *Polarizers and Applications*, vol. 307 (SPIE, 1982), pp. 120–125.

14. T. Zhang, D. Popov, and M. Khodzitsky, "Terahertz achromatic quarter-wave plate composed of quartz and mgf 2," in *2021 46th International Conference on Infrared, Millimeter and Terahertz Waves (IRMMW-THz)*, (IEEE, 2021), pp. 1–2.
15. M. Born and E. Wolf, *Principles of optics: electromagnetic theory of propagation, interference and diffraction of light* (Elsevier, 2013).
16. S. A. Teukolsky, B. P. Flannery, W. Press, and W. Vetterling, "Numerical recipes in c," *SMR* **693**, 59–70 (1992).
17. D. Grischkowsky, S. Keiding, M. Van Exter, and C. Fattinger, "Far-infrared time-domain spectroscopy with terahertz beams of dielectrics and semiconductors," *J. Opt. Soc. Am. B* **7**(10), 2006–2015 (1990).